UC Santa Barbara
UC Santa Barbara Previously Published Works

Title

3D Columnar Phase of Stacked Short DNA Organized by Coherent Membrane Undulations

Permalink

https://escholarship.org/uc/item/7fs1m1kz

Journal

Langmuir, 35(36)

ISSN

0743-7463

Authors

Bouxsein, Nathan F
Leal, Cecília
McAllister, Christopher S
et al.

Publication Date

2019-09-10

DOI

10.1021/acs.langmuir.9b01726

Copyright Information

Peer reviewed

A 3D columnar phase of stacked short DNA organized by coherent membrane undulations

Nathan F. Bouxsein[1], **Cecília Leal**[2], **Christopher S. McAllister**[3,§], **Youli Li**[4], **Kai K. Ewert**[1], **Charles E. Samuel**[3], **Cyrus R. Safinya**[1,*]

[1]Materials Department, Physics Department, Molecular, Cellular, and Developmental Biology Department, University of California, Santa Barbara, California 93106, USA

[2]Department of Materials Science and Engineering, University of Illinois Urbana-Champaign, Urbana, IL 61801, USA

[3]Molecular, Cellular, and Developmental Biology Department, University of California, Santa Barbara, California 93106, USA

[4]Materials Research Laboratory, University of California, Santa Barbara, California 93106, USA

Abstract

We report on the discovery of a new organized lipid-nucleic acid phase upon intercalation of blunt duplexes of short DNA (sDNA) within cationic multilayer fluid membranes. End-to-end interactions between sDNA leads to columnar stacks. At high membrane charge density, with the inter-sDNA column spacing (d_{sDNA}) comparable but larger than the diameter of sDNA, a 2D columnar phase (i.e. a 2D smectic) is found similar to the phase in cationic liposome-DNA complexes with long lambda-phage DNA. Remarkably, with increasing d_{sDNA} as the membrane charge density is lowered, a transition is observed to a 3D columnar phase of stacked sDNA. This occurs even though direct DNA-DNA electrostatic interactions across layers are screened by diffusing cationic lipids near the phosphate groups of sDNA. Softening of the membrane bending rigidity (κ), which further promotes membrane undulations, significantly enhances the 3D columnar phase. These observations are consistent with a model by Schiessel and Aranda-Espinoza where local membrane undulations, due to electrostatically-induced membrane wrapping around sDNA columns, phase lock from layer-to-layer, thereby precipitating coherent "crystal-like" undulations coupled to sDNA columns with long-range position and orientation order. The finding that this new phase is stable at large d_{sDNA} and enhanced with decreasing κ is further supportive of the model where the elastic cost of membrane deformation per unit area around sDNA columns ($\propto \kappa h^2/d_{sDNA}^4$, h^2 = sum of square of amplitudes of the inner and outer monolayer undulations) is strongly reduced relative to the favorable electrostatic attractions of partially wrapped membrane around sDNA columns. The findings have broad implications in the design of membrane-mediated assembly of functional nanoparticles in 3D.

Graphical Abstract

---

[*]Corresponding author contact information: safinya@mrl.ucsb.edu.
[§]Present Address: Genomics Institute of the Novartis Research Foundation, San Diego, CA 92121, USA

3D Phase-Locked Fluid Membrane Undulations
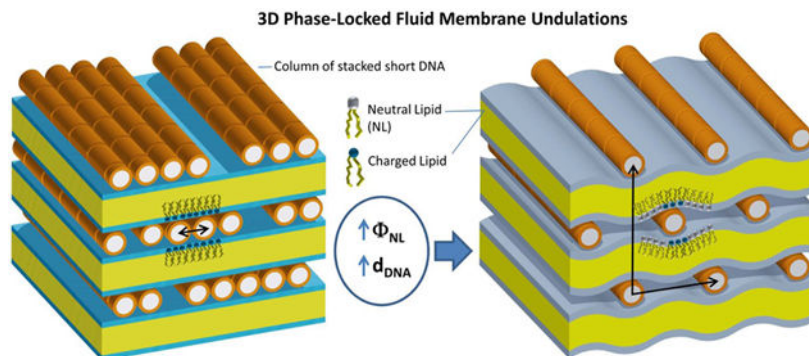
Keywords

Stacked short-DNA; columnar phase; 3D membrane undulations; synchrotron SAXS

INTRODUCTION

Self-assembled complexes of cationic liposomes (CLs) and nucleic acids (NA) have been of significant interest to the field of nucleic acid nanomaterials. This, in part, is because of the ability to organize DNA and RNA in three-dimensional (3D) space in a variety of geometries with distinct lattice symmetries due to the electrostatic coupling of nucleic acids to charged membranes (1–18). Distinct CL-NA structures revealed by synchrotron x-ray diffraction include the lamellar L_α^C with DNA sandwiched between cationic membranes (1,10); the inverted hexagonal H_{II}^C with DNA or stacked short DNA encapsulated within inverse lipid tubules (3,15); and the H_I^C structure, where cationic multivalent lipids with large positive spontaneous curvature lead to hexagonally arranged rod-like micelles surrounded with DNA chains forming a continuous substructure with honeycomb symmetry (11). For short double-stranded RNA, bicontinuous cubic phases, including the gyroid $Q_{II}^{G, NA}$, may be realized containing the RNA molecules on curved surfaces with negative Gaussian curvature (13,16–18). In addition to the scientific interest arising from the different structural arrangements of nucleic acids on membrane templates, CL-NA complexes are also of high biomedical interest because of their applications in delivery of therapeutic nucleic acids, both DNA (19–32) and short RNA (13,16–20,23,26,27,29–31,33–42) into cells. The high level of research interest in CL–NA complexes is complemented with more than 110 ongoing gene therapy trials worldwide using CL based carriers (vectors) (43,44).

The precise nature of long DNA chains confined between cationic bilayer sheets in the lamellar L_α^C phase has been well elucidated through careful line-shape analysis of the structure factor obtained by synchrotron x-ray scattering. These analyses show that DNA chains form a finite-sized 1D lattice on the scale of the persistence length of DNA ($\xi_p \approx 500$ Å to 1000Å) with weak cross bilayer correlations (45,46). Thus, DNA chains in each two-dimensional (2D) layer are nearly decoupled 2D smectics (or equivalently a 2D columnar phase) on length scales up to $\approx \xi_p$.

For long DNA, modeled as rigid rods confined between flat bilayer membranes, equilibrium theories have described a 3D columnar phase where DNA rods have long-range positional

and orientational correlations across the bilayers (4,5,9). The models also predict a new phase of matter, which remains to be observed in experiments, referred to as a "sliding columnar" phase where DNA rods forming a 2D columnar phase lose positional correlations between bilayers but maintain 3D long-range (LR) orientational order. It is important to emphasize that in these models describing DNA arrangements on flat lipid bilayers, membrane undulations play no role in the equilibrium properties of the phases. Thus, long-range repulsive electrostatic forces between DNA rods in different layers stabilizes the 3D columnar phase.

In this paper, we combined cationic liposomes (CLs) consisting of mixtures of the cationic lipid 1,2-dioleoyl-3-trimethylammonium-propane (DOTAP) and neutral lipid 1,2-dioleoyl-sn-glycero-3-phosphocholine (DOPC) with blunt short DNA (sDNA) consisting of either 11bp, 24bp or 48bp. Both lipids are in their chain-melted conformation forming fluid (i.e. liquid state) membranes in the temperature range studied (ambient room temperature to $\approx$ 80 °C). Synchrotron x-ray scattering experiments show that all three lengths of blunt sDNA form lamellar complexes with sDNA intercalated between the lipid bilayers. DNA-DNA correlations can be clearly elucidated from the scattering data revealing two highly organized arrangements of sDNA. These organization are only possible if sDNA rods stack end to end to form long columns (see Fig. 1A). This is consistent with a previous study that established blunt duplexes of sDNA in water preferentially stack end-to-end, forming sDNA columns to minimize exposure of the hydrophobic ends of the duplex to the aqueous environment (47,48). Finally, the analysis of short pieces of DNA with nonpairing overhangs adsorbed on 2D membranes has found that tuning of end-to-end stacking interactions, by altering number of the nonpairing overhangs, results in finite length stacks of sDNA (14).

For CL-sDNA complexes formed at low mole fraction neutral lipid (Φ_{NL}), stacked sDNA sandwiched between cationic membranes form columns with a well-defined DNA interaxial spacing in each layer with no indication of correlations from layer to layer. This 2D columnar phase of stacked sDNA (labeled $L_\alpha^{sDNA,2D}$, Fig. 1A, left) is qualitativly similar to the 2D smectic-like organization of long DNA in cationic liposome-DNA complexes of previous reports (1,45,46). The main difference is that while the persistence length of DNA ($\xi_p \approx 500$ Å to 1000Å) sets the length scale for the 2D smectic domains of long DNA in the L_α^C phase (i.e. with exponentially decaying in-plane orientational correlations between domains on scales larger than ξ_p), the columns of sDNA are expected to be much longer than ξ_p in the $L_\alpha^{sDNA,2D}$ phase. With increasing Φ_{NL} ($0.5 < \Phi_{NL}$ 0.75 for 11bp and 24bp sDNA, and $0.52 < \Phi_{NL}$ 0.75 for 48bp sDNA), we observed strong correlations across bilayers through the onset of a series of new diffraction peaks indicative of long-range order in position and orientation of sDNA columns. This 3D columnar phase of stacked sDNA, labled $R_\alpha^{sDNA,3D}$, indexes onto a 2D centered rectangular phase (Fig. 1A, right). We stress that this is the first time a highly organized sDNA lattice with long-range position and orientation order has been seen in lipid-NA complexes comprised of *fluid membranes.*

3D columnar phases of long DNA in lipid-DNA complexes have been reported in systems where the membrane is in the ordered gel phases with chain-frozen lipids (49–51). In the gel phase the very high membrane bending rigidities ($\kappa \gg k_B T$) effectively suppress thermal undulations giving rise to flat membranes. Furthermore, because of chain ordering, cationic

lipids have limited mobility and provide little screening of coulombic forces between DNA rods in different layers. Therefore, columnar ordering occurs due to mutual DNA-DNA repulsions. Our observation of 3D long-range order of sDNA columns confined between fluid membranes, with lipids in their chain-melted conformation, is highly unexpected. This is because direct electrostatic DNA-DNA interactions are expected to be short-range due to screening by liquid-like cationic lipids in the vicinity of the phosphate groups of DNA. Unlike the case for chain ordered membranes with large κ, the 3D columnar phase of stacked sDNA described in this paper is strongly enhanced with decreasing κ, which promotes membrane undulations. As described later, this points to a different origin of ordering where coherent membrane undulations across layers (Fig. 1A, right) trigger the onset of long-range 3D positional and orientational columnar ordering.

The findings of this paper have broader implications in the area of assembly in biological nanomaterials. Many of the prevailing approaches in hierarchical assembly of nanoscale building blocks involve either specific interactions, such as H-bonding of complementary nucleic acid base pairs attached to colloidal nanoparticles (52–55), or nonspecific electrostatic interactions, for example, between intrinsically disordered protein biopolymers bound to the surface of other structured proteins (56–58). Here we used the mutual electrostatic coupling of short sDNA rods and flexible membranes as the mechanism for 3D ordering of sDNA. The method may be extended to other nanoparticles of different shape with a designed-in coupling to membranes; for example, charged peptide rods with built in end-end hydrophobic interactions, both for structure studies (e.g. fiber diffraction) and as advanced materials in applications requiring a local high concentration such as biosensing.

MATERIALS AND METHODS

DNA Constructs.

All DNA constructs were purchased as single strands from Sigma-Genosys (Sigma-Aldrich) and delivered as a lyophilized film. All oligos where fully deprotected, leaving hydroxy 5′ ends, and desalted. HPLC was used for oligos > 30 nts (nucleotides). The films were centrifuged to collect all dried components and then resuspended in 10mM HEPES buffer (pH = 7.0) to > 10mg/ml. Concentrations were determined by UV-Vis absorption using a ND-1000 UV-Vis spectrophotometer from NanoDrop Technologies (Thermo Fisher Scientific). Equimolar amounts of complimentary single strands were mixed and diluted to a final concentration of 10mg/ml. Mixed single strands were heated in a water bath and held at 90 C for 15 min. The nucleci acids were then slow cooled to room temperature to facilitate complete hybridization. Duplexes were run on a 12% polyacrylamide gel to check for ssDNA contaminates. DNA sequences are listed in Table S1 (Supporting Information). Control sequences of DNA homopolymers, polydeoxyadenylate and poldeoxythymidylate, were purchases at lengths of 11nts, 24nts and 48nts (Sigma-Genosys) and hybridized or left as single strands.

Lipid Preparation.

1,2-dioleoyl-3-trimethylammonium-propane (DOTAP) and 1,2-dioleoyl-sn-glycero-3-phosphocholine (DOPC) lipids were purchased from Avanti Polar Lipids (Alabaster,

Alabama) and delivered as lyophilized powders. Liposome solutions were prepared by dissolving DOTAP and DOPC in trichloromethane to stock concentrations of 30mM respectively. Stock concentrations were mixed at molar ratios (DOTAP:DOPC) of 100:00, 80:20, 40:60 and 30:70 into glass vials (corresponding to Φ_{NL} = 0, 0.2, 0.6 and 0.7 respectively). Trichloromethane mixtures of lipids where then dried under a stream of nitrogen to produce a dried lipid film inside the vial. Dried films were then placed under vacuum for 24 hours. Films were then rehydrated in ultra pure water to a final concentration of 30mM and incubated at 37 C. Liposome solutions were sonicated with with a Vibra-Cell (Sonics & Materials, Inc. Newtown, CT) tip sonicator for 10 min and immediately stored at 4 C until use.

Complexes for X-ray.

Complexes for x-ray diffraction were prepared as described previously (12,14). Briefly, 50 μg solutions of DNA or RNA were alloquoted into x-ray quartz capillaries (Hilgenberg, Malsfeld Germany). Lipid mixtures were added at $moles_{CL} = \frac{N_{nt}^{NA}}{z_{cL}} \times \rho_{chg} \times \frac{50\mu g}{MW_{NA}}$ where N_{nt}^{NA} are the total nucleotides in the DNA or RNA duplex, Z_{CL} is the cationic lipid headgroup charge (= +1e for DOTAP) and ρ_{chg} is the molar charge ratio between CL:NA for the complex. We set ρ_{chg} = 1 such that all complexes tested were isoelectric (each negative charge on DNA is compensated by one positively charged lipid). After adding appropriate lipid mixtures, capillaries were spun at $1,500 \times g$ for 15 min at 4 C to pellet the condensed aggregate. Capillaries were sealed and stored at 4 C until use. X-ray diffraction experiments were preformed at Stanford Synchrotron Radiation Lightsource beam line 4–2 using a 1.5 meter flight path with x-ray energy set to 9keV. Data was collected on MX-225 Rayonics (Evanston, IL) CCD detector and radially averaged to produce 1D intensity vs wavevector (**q**) plots. Before diffraction experiments, samples were either incubated at 37 C for 6 hours or left at 4 C. Some diffraction experiments were preformed under temperature control using a custom oven with Minco (Minneapolis, MN) heaters and accuracy ± 0.2 C. In these samples the temperature was measured by a thermister, which was in thermal contact with the sample holder.

RESULTS AND DISCUSSION

The 2D Columnar Phase of Stacked sDNA (labled Lα^sDNA,2D) in Cationic Liposome-sDNA Complexes.

Figure 1B(i) shows synchrotron x-ray scattering data of 11bp sDNA complexed with DOTAP/DOPC CLs for Φ_{NL} = 0.2 at the isoelectric point of the complex (i.e. where the number of negative phosphate groups from sDNA equals the number of cationic charges from DOTAP). The series of peaks at (00L) (L = 1,2,3...) results from the multilamellar structure of the complexes with inter-membrane spacing d = $2\pi/q_{001}$ = $2\pi/(0.104$ Å$^{-1})$ = 60.4 Å (Fig. 1A, left). The inter-membrane distance (d) was obtained by fits of the profiles to Lorentzian line-shapes. The inter-membrane distances are very similar to what is obtained when sDNA is replaced with long (48,502 bp) lambda-phage where d (= $\delta_m + \delta_w$) is the thickness of the lipid bilayer membrane (δ_m = 35 +/− 0.5 Å) plus the water layer ($\delta_w \approx 25$

Å) containing a layer of sDNA (sDNA in the hydrated B-conformation has a physical diameter ≈ 20Å) (1,45,46).

The broader highly asymmetric peak observed between the (002) and (003) peaks (labeled q_{sDNA} at 0.239 Å^{-1}) is strikingly similar, both in shape and peak position at the same Φ_{NL}, to the diffraction peak from the 1D lattice of DNA chains (i.e. a 2D smectic) observed previously for lamellar phase CL-DNA complexes formed with long lambda-phage DNA (45,46). The strong asymmetry, where the lineshape has a sawtooth shape rising rapidly and falling off slowly after the peak position, is a well-known signature of powder averaged anisotropic x-ray structure factor of a 1D lattice of rods in two-dimensions (45). Taken together, the comparison to scattering from long DNA in lamellar complexes indicates that sDNA molecules, confined between lipid bilayers, are stacked end-to-end forming long columns with well-defined inter-column spacing (for the data in Fig. 1B(i) $d_{sDNA} = 2\pi/q_{sDNA} = 26.3$ Å at $\Phi_{NL} = 0.2$). The strong asymmetric lineshape is also a direct indication that the positional correlations of the 1D lattices across layers is short-range (46). Thus, at $\Phi_{NL} = 0.2$ cationic liposome-sDNA complexes form a 2D columnar phase of stacked sDNA ($L_\alpha^{sDNA,2D}$). Interestingly, long DNA and sDNA complexes differ only in the line widths of the DNA peak, which are inversely proportional to the coherent domain sizes of the respective 1D lattices and are obtained from the rapidly rising part of the DNA-DNA lineshape, which is not affected by the powder averaging process in the lineshape analysis (45,46). Using Lorentzian lineshapes for the structure factor one finds that at $\Phi_{nl} = 0.2$ the 1D lattice of sDNA columns has a larger coherent domain size ≈ 460 Å (≈ 18 times the unit cell dimension) by about a factor of four compared to the that for long DNA (1,45,46). This finding is consistent with the length of the sDNA columns being significantly larger than the persistence length of DNA, which sets the scale for the domain size of 1D lattices of DNA chains.

We should point out that the stacking of blunt sDNA adsorbed on lipid bilayers is not unexpected because such stacking has been previously observed when sDNA is in aqueous solution (47,48). Blunt DNAs have an exposed hydrophobic core at each end, an unfavorable situation in the aqueous environment between bilayer membranes. In B-form DNA, the base pairs are nearly perpendicular to the longitudinal axis of the DNA strands. Therefore, stacking of blunt DNA ends will put adjacent DNA molecules in near perfect contact, allowing for greater stability by protecting the hydrophobic core of bases and creating further π-π bonding of the end base's aromatic groups. These non-covalent interactions would "glue" the blunt DNA together creating stacks. A similar case has been reported for the stacking of aromatic dye molecules into columns (59).

To further prove the stacking nature of the blunt sDNA, we created complexes with an identical DNA core (11 bp, perfectly duplexed) but including 10 unpaired deoxythymidine nucleotides to each 3' end of the duplex (labeled 11DNA-10dT). Diffraction data of 11DNA-10dT complexes at $\Phi_{NL} = 0.2$ are shown in Fig. 1B(ii). Interestingly, a very broad peak at $q_{DNA} = 0.218$ Å^{-1} can be seen for this sample ($\Phi_{NL} = 0.2$) indicative of a disordered (isotropic) phase of unstacked duplexes. The addition of 10dT dangling incompatible single stranded ends prevent end stacking. For comparison, complexes made with a single-stranded homopolymer of deoxythymidine are included in Figure 1B(iii). These complexes with

single-starnded 11dT DNA show no indication of any correlation peak. The value of q_{001} for the ssDNA poly(dT) shifts to larger q values compared with the dsDNA analog (compare Fig. 1B(iii) to (i)) indicative of a smaller unit cell normal to the layers. Since lipid composition remains constant between these samples, δ_m must remain fixed and therefore, δ_w which contains the 11dT is smaller with the introduction of ssDNA.

The 3D Columnar Phase of Stacked sDNA (labled $R_a^{sDNA,3D}$) in Cationic Liposome-sDNA Complexes.

At higher neutral lipid compositions ($\Phi_{NL} > 0.50$ for 11bp and 24bp sDNA and $\Phi_{NL} > 0.52$ for 48bp sDNA) x-ray scattering data from CL-sDNA complexes shows a phase transition to a new phase with the onset of new diffraction peaks. Figure 1B(iv) depicts a typical scattering profile in this new phase for 11bp sDNA at $\Phi_{NL} = 0.64$ where the sharp peaks, from the diffraction of the sDNA columns within the lipid bilayers, index to a center rectangular columnar structure with peak positions at reciprocal lattice vector $G_{hk} = 2\pi[(h/a)^2 + (k/b)^2]^{1/2}$ with the 2D lattice parameters **a** (= sDNA intercolumn spacing = 45.9 Å at $\Phi_{NL} = 0.64$) and **b** (= 2*interlayer spacing d = 138.8 Å at $\Phi_{NL} = 0.64$) as indicated in Figure 1A (right). The observable (h,k) peaks [(02), (11), (04), (13), (15), (06), (08)] all satisfy the condition that h plus k equal an even number as required for a body centered rectangular lattice. Furthermore, the observation of the 2D center rectangular lattice implies that the sDNA columns have long-range position and orientation order within the 3D multilayer system; that is, a 3D columnar phase of stacked sDNA, which we have labeled $R_a^{sDNA,3D}$ (Fig. 1A, right). To our knowledge, this is the first time this configuration has been seen in lamellar CL-NA systems with *fluid* membranes (the subscript "alpha" in the label denotes the liquid state of the membrane due to chain-melted lipids).

In figure 1B (v, vi) comparison diffraction data for CL-DNA complexes with 11DNA-10dT and 11-base single stranded deoxythymidine (11dT) are shown, respectively. In both cases, the data show no peaks from ordered rectangular phase. This result confirms that end-to-end stacking of short blunt sDNA into long columns is required for forming both 2D ($L_a^{sDNA,2D}$) and 3D columnar phases ($R_a^{sDNA,3D}$).

Phase Behavior of Stacked sDNA Columns in Cationic Liposome-sDNA Complexes as a Function of Neutral Lipid Composition.

Figure 2A depicts the complete series of synchrotron x-ray scattering profiles of CL-sDNA complexes for 11bp sDNA as a function of increasing Φ_{NL} covering the range from $\Phi_{NL} = 0.2$ to $\Phi_{NL} = 0.8$ (at the isoelectric point of the complex). A plot of a subset of the x-ray profiles over a smaller q-range for Φ_{NL} between 0.54 and 0.70 is shown in figure 2B. This latter figure more clearly shows the extra diffraction peaks of the $R_a^{sDNA,3D}$ phase absent in the $L_a^{sDNA,2D}$ phase; that is, the (13) peak (solid arrow) for $\Phi_{NL} = 0.54$ to 0.64, and the (15) peak (dashed arrow) for $\Phi_{NL} = 0.64$, 0.65, and 0.70. The transition from a 2D columnar phase ($L_a^{sDNA,2D}$) to a 3D columnar phase of stacked sDNA ($R_a^{sDNA,3D}$) occurs between $\Phi_{NL} = 0.50$ and $\Phi_{NL} = 0.52$ (where the (13) peak is weak but visible).

The stability regime for the $L_a^{sDNA,2D}$ and $R_a^{sDNA,3D}$ phases as a function of Φ_{NL} for CL-sDNA complexes with 11DNA, 24DNA and 48DNA is shown in the phase diagram plot in

figure 2C. All three lengths of blunt DNA generally behave the same. For Φ_{NL} 0.50 for 11DNA and 24DNA and Φ_{NL} 0.52 for 48DNA, CL-sDNA complexes are in the 2D columnar phase ($L_\alpha^{sDNA,2D}$). Here, the diffraction patterns (Fig. 2A) are strikingly similar to the case of CL-DNA complexes formed with long linear λ-DNA (i.e. the L_α^C phase with DNA sandwiched between cationic membranes (1) where one observes a highly asymmetric DNA peak significantly broader than the (00L) layering peaks. CL-DNA complexes with λ-DNA remain in the L_α^C phase. They do not exhibit a transition to the 3D columnar phase over the entire range of Φ_{NL} between 0 and 0.75 beyond which, the L_α^C phase separates with a lamellar phase with no DNA (45,46) (Fig. 2C, blue triangles). In contrast the 3D columnar phase of stacked sDNA (black squares) occupies a signficant fraction of the phase diagram for larger Φ_{NL} ($0.5 < \Phi_{NL}$ 0.75 for 11bp and 24bp sDNA, and $0.52 < \Phi_{NL}$ 0.75 for 48bp sDNA). For even larger Φ_{NL} all diffraction peaks broaden and are indicative of the 3D columnar phase but with smaller domain sizes (0.80 and 0.85 profiles in Fig. 2A).

We found that annealing the CL-sDNA complexes formed at room temperature by incubation at 37°C for six hours followed by slow cooling to room temperature tended to sharpen the observed diffraction peaks in the $R_\alpha^{sDNA,3D}$ phase due to annealing of defects resulting in larger coherent domains. This makes the additional higher order peaks associated with the rectangular phase more clearly visible (see supplementary Fig. S1). The incubation period at elevated temperature promotes the dynamics of the short DNAs in order to increase the number of end to end collisions required for stacking. All room temperature samples leading to the phase diagram in figure 2C were subject to temperature annealing. For long lambda-DNA, CL-DNA complexes do not show any significant narrowing of diffraction peaks upon incubation and no evidence of the $R_\alpha^{sDNA,3D}$ phase is found as a function of varying Φ_{NL}.

Figure 3 summarizes the structural parameters derived from the synchrotron x-ray scattering data from CL-sDNA complexes for 11bp (A), 24bp (B), and 48bp (C) sDNA as a function of Φ_{NL} in the $L_\alpha^{sDNA,2D}$ and $R_\alpha^{sDNA,3D}$ phases. This includes the average spacing between sDNA molecules (dsDNA and lattice parameter **a**) and the interlayer spacing (d and **b** = 2*interlayer spacing) in the $L_\alpha^{sDNA,2D}$ and $R_\alpha^{sDNA,3D}$ phases, respectively (see Fig. 1A). We see that d_{sDNA} and **a** increase with increasing Φ_{NL} increases. Thus, the increase in Φ_{NL} from 0 to 0.7 leading to a decrease in the average membrane charge density forces sDNA columns to be further apart. This trend is also observed with CL-DNA containing long λ-DNA (1). This behavior is due to the fact that within the CL-sDNA complex the average anionic charge density due to the sDNA has to match the average membrane charge density because of the requirement of local charge neutrality assuming all counter-ions of the phosphate groups and the cationic lipid headgroup have been released from the complex into the surrounding solution (1,60). Figure 3 also shows that the interlayer spacing (d and **b/2**) equal to δ_M plus δ_w increases with increasing Φ_{NL}. This behavior is due to increases both in the membrane bilayer thickness δ_M (each DOPC molecule is ≈ 4 Å to 6 Å longer than a DOTAP molecule) and the water layer as Φ_{NL} increases because DOPC has a larger hydration shell compared to DOTAP) (1,20).

Decrease in the Membrane Bending Rigidity κ Enhances the 3D Columnar Phase in Cationic Liposome-sDNA Complexes (R$_\alpha^{sDNA,3D}$).

To better understand the effect of membrane bending rigidity (κ) on the stability of the R$_\alpha^{sDNA,3D}$ phase, we added the membrane soluble co-surfactant hexanol to the lipid mixture prior to complexation with the short DNA for a CL-sDNA complex at $\Phi_{NL} = 0.7$ well in the R$_\alpha^{sDNA,3D}$ phase. While co-surfactant molecules, which typically consist of long-chain alcohols (e.g. pentanol, hexanol, heptanol), are not able to stabilize an interface separating hydrophobic and hydrophilic regions, when mixed in with longer chain surfactants they are known to lead to dramatic changes in interface elasticities. Compressional models of surfactant chains (61) show that the bending rigidity (κ) scales with the membrane thickness $\kappa \propto \delta_m^P$ with P between 2 and 3. The mixing of co-surfactants with lipids is expected to lead to a thinner membrane and a strong suppression of κ making the membrane highly flexible. Indeed, previous x-ray scattering experiments have shown that the addition of co-surfactants like pentanol, hexanol, and heptanol to lipid membranes of lamellar phases with a mole ratio of between ≈ 3 to ≈ 6 (i.e. where long chain lipids are effectively surrounded by much shorter chain co-surfactants) leads to a significant decrease of k from ≈ 10 to k_BT to ≈ 2–3 k_BT (62).

In our studies we added hexanol at a 5:1 molar ratio to total lipid. Figure 4 compares the x-ray scattering profile of CL-sDNA complexes in the R$_\alpha^{sDNA,3D}$ phase with no added hexanol (bottom) to one with added hexanol (top). One can see immediately that the profiles for complexes with softer membranes display a significant sharpening of the peaks. The narrowing of the diffraction peaks implies larger coherent domains sizes and the presence of longer columns of stacked sDNA) due to softening of the membranes. The larger domain sizes readily leads to observation of additional peaks, in particular, the (20) and (22) of the centered rectangular lattice of sDNA columns, which were buried under the tail scattering of the wider peaks of the x-ray profiles of complexes with no added hexanol. We also note that the (13) peak which appears as a shoulder before the (04) peak is clearly visible in complexes containing hexanol. What is even more remarkable is that whereas the samples with no added hexanol benefited from incubation at 37 °C for six hours (as discussued in the previous section), no incubation at elevated temperature was required for the samples with softer membranes and very sharp diffraction peaks of the R$_\alpha^{sDNA,3D}$ phase were immediately apparent with no temperature annealing (Fig. 4 top). As we discuss below this result is consistent with the fact lowering the rigidity of fluid membranes by decreasing κ should favor the formation of the R$_\alpha^{sDNA,3D}$ phase consisting of coherent membrane undulations from layer-to-layer.

Effect of Temperature on Stacked sDNA Columns in Cationic Liposome-sDNA Complexes.

The requirement of an incubation step at elevated temperature prompted us to study the CL-sDNA complexes as a function of temperature. The experiments were performed in-situ by using a temperature controlled sample chamber (oven). The oven containing the sample typically reached equilibrium in about 5 minutes, however, each sample was held at the indicated temperature for 15 minutes prior to x-ray exposure to ensure that the sample had reached equilibrium, which was further confirmed where subsequent x-ray exposure at a later time did not change the x-ray scattering profile. Scattering profiles were found to be

fully thermally reversible upon slow cooling with peak line widths returning to their original room temperature values.

Figure 5 (A) depicts x-ray scattering data plotted as a function of increasing temperature for CL-sDNA complexes with 11bp DNA in the $R_\alpha^{sDNA,3D}$ phase at $\Phi_{NL} = 0.6$. The right panel (Fig. 5B) shows an expanded view of the x-ray profiles over a smaller q-range where the (13) peak (see arrows) of the 3D columnar phase (melted in the 2D columnar phase) is more clearly visible. It is clear from the data that the $R_\alpha^{sDNA,3D}$ phase is the dominant phase in the lower temperature range (T = 28°C to 44.6 °C), where the (13) difftraction peak indicative of 3D columnar organization remains relatively narrow. This is compared to a lamellar phase (56.1 °C to ≈ 69.3 °C), where the (13) peak characteristic of the 3D columnar phase is melted and where the sharper (11) peak of the $R_\alpha^{sDNA,3D}$ phase is replaced by a broader q_{sDNA} indicative of the $L_\alpha^{sDNA,2D}$ phase. On closer inspection one can see that the q_{sDNA} peak appears as a shoulder to the (11) peak beginning from T = 39.5 °C (dashed arrow) and is the main broader peak by T = 56.1 °C (Fig. 5B). CL-sDNA complexes consisting of 24 bp and 48 bp DNA at $\Phi_{NL} = 0.6$ show similar temperature dependent behavior with the (13) peak replaced by a broad diffuse peak by T = 48.9 °C. Upon further increases in temperature (75.2 °C to 77.9 °C) the q_{sDNA} peak broadens and vanishes beyond 85.2 °C.

Figure 6 plots the lamellar lattice spacing (membrane bilayer plus a water layer containing the sDNA columns) as a function of increasing temperature. We see that the spacing decreases smoothly up to about 75 °C for both 11 bp sDNA and 48 bp sDNA complexes. This decrease is due to thermal contraction of the lipid chains. Beyond 75 °C, we see that both duplexes begin to show a more rapid decrease in lattice spacing with increasing temperature, with the decrease being much larger for complexes with the 11 sDNA duplexes. This additional decrease is due to the onset of duplex sDNA denaturation, which would lead to the observed more rapid rate of decrease in the lamellar lattice spacing with increasing temperature where the monolayer of duplex sDNA is replaced by a mixture of denatured single-strand short DNA and double stranded sDNA. Denaturation would also lead to breakup of the end-to-end interaction and disruption of sDNA columns. This is consistent with the SAXS data of Fig. 5 where the qsDNA peak is very weak at 77.9 °C and entirely absent at 85.2 °C and 89.9 °C.

Returning to the profiles at T = 48.9 °C and 51.4 °C, we note that the narrow (13) peak is replaced by a broader diffuse scattering peak (more so for the sample at 48.9 °C than 51.4 °C). This is indicative of short range positional order between columns from layer to layer absent in the higher temperature profiles in the 2D columnar phase (56.1 °C to 69.3 °C) with no hint of diffuse scattering near the (13) peak position. The phase in this intermediate temperature range (≈ 48.9 °C to ≈ °51.4 °C) between the $R_\alpha^{sDNA,3D}$ phase and the $L_\alpha^{sDNA,2D}$ phase may indeed be a good candidate for the theoretically predicted sliding columnar phase where the 2D columns in each layer (with finite in-plane compressibility modulus) readily slide pass each other in neighboring layers, indicative of short range positional order across layers, but where the columns have 3D long range orientational order (4,5,9).

Origin of Long-Range 3D Positional and Orientational Correlations of the Columns of Stacked sDNA in Cationic Liposome-sDNA Complexes.

A central question related to our findings is the origin of 3D long-range positional and orientational correlations of the columns of sDNA, given that direct DNA-DNA electrostatic interactions from layer-to-layer are expected to be short-ranged due to screening by the cationic lipids diffusing in the liquid phase of the membrane in the vicinity of sDNA phosphate groups. Our experimental findings are consistent with the theoretical model of Schiessel and Aranda-Espinoza on layered lipid-DNA complexes. Under equilibrium conditions, coupling of membrane undulations along the stacking direction promotes coupling of DNA rods in different layers (63,64). In their model undulations are initiated by the electrostatic wrapping of cationic lipid membranes around long DNA rods. Furthermore, coherent membrane undulations with wavelength $\lambda = d_{sDNA}$ (inter-sDNA column spacing, see Fig. 1A, right) are more favorable at large DNA interaxial spacing because of a significantly lower elastic cost. This is consistent with our experimental finding of long-range 3D positional and orientational order of sDNA columns at high Φ_{NL} (i.e. large d_{sDNA}).

This may be seen in a calculation of the elastic cost of a sinusoidal membrane undulation along the x-axis partially wrapped around sDNA columns pointing along the y-axis (Fig. 1A, right). In this model one may separately consider sinusoidal undulations of the outer and inner monolayers with amplitudes h_i and h_o, respectively, where $h_i = fa$ (a = radius of sDNA, f = constant < 1 is a measure of the degree of membrane wrapping around sDNA columns) and $h_o = h_i + \delta_m$ (see supplemental section). For each layer one may write $h_{o,i}(x) = h_{o,i} \sin(qx)$, with wavevector $q = 2\pi/\lambda = 2\pi/d_{sDNA}$ (see Fig. 1A, right). Using the Helfrich model of curvature elasticity of a fluid membrane (65) we find that the elastic cost per unit area of a membrane bilayer undulation is $\propto \kappa h^2 q^4 \propto \kappa h^2/\lambda^4 = \kappa h^2/d_{sDNA}^4$, where $h^2 = h_i^2 + h_o^2$ (65). Thus, the rapid decay of elastic cost with increasing inter-sDNA column spacing implies that for large enough d_{sDNA}, the elastic cost of membrane deformation may be expected to be smaller than the gain in attractive electrostatic energy due to partial membrane wrapping. This would lead to a stable 3Dn columnar phase of stacked sDNA (i.e. the $R_\alpha^{sDNA,3D}$ phase).

Our finding that decreases in the membrane bending rigidity, through addition of the co-surfactant hexanol to the fluid membranes, strongly enhances the domain size of the $R_\alpha^{sDNA,3D}$ phase, is further confirmation of the model where coherent undulation modes giving rise to 3D columnar ordering, is favored by low κ (63). Thus, long-range position and orientation order of undulations within the multilayer system; that is, "crystallized undulations" provides a natural mechanism driving the onset of the 3D columnar phase (Fig. 1A, right).

Taken together, our results strongly suggest that the absence of the 3D columnar phase in CL-DNA complexes with long lambda-phage DNA (1,10,45,46) results from the fact that the DNA chain cannot be viewed as a model of long rigid rods but rather, on length scales larger than the DNA persistence length between 50 nm to 100nm, as a meandering flexible rod. Thus, the 3D columnar phase is not expected to be energetically favorable because the "random" local orientation of long DNA chains is expected to be uncorrelated between layers. In contrast, CL-sDNA complexes exhibit the 3D columnar phase precisely because

upon stacking they are good models of very long rigid rods and thus the undulations of one layer may be coherent with other layers over very large membrane areas. Thus, somewhat counterintuitively, short blunt sDNA, which stacks to produce long rigid rods, provides a better experimental model of current theoretical models of rigid rods sandwiched between membranes (63,64,4,5,9) compared to long lambda-phage DNA.

Our hypothesis on why the 3D columnar phase is absent in CL-DNA complexes with long lambda-phage DNA implies that as one increases the length of the blunt sDNA molecule there will be a length beyond which the new 3D columnar phase reported here will not exist. In fact we expect this to correspond to sDNA molecules that no longer behave as rigid rods but rather exhibit one or two bends with distances between bends being of order the persistence length of DNA.

CONCLUSIONS

3D columnar phases of long DNA confined between membranes in lipid-DNA complexes have been reported in systems where the flat membranes are in the chain-frozen ordered phase with very high bending rigidities ($\kappa \gg k_BT$). This is in contrast to our observation of a 3D columnar phase of stacked short blunt DNA duplexes in flexible fluid multilayer membranes, which, in turn, is further enhanced as the bending rigidity is lowered by addition of co-surfactant. Chain frozen cationic lipids with no demixing provide little screening of coulombic forces between DNA rods in different layers and columnar ordering may occur due to mutual DNA-DNA repulsions. In contrast, our observations are consistent with coherent macroscopic membrane undulations, electrostatically coupled to sDNA columns, as the mechanism of inducing long-range position and orientation order of the columns. This new phase of soft matter may be thought of as a 3D crystal of membrane undulations with repeating unit cell, consisting of a curved membrane ribbon coupled to a column of sDNA with width equal to the DNA-DNA interaxial distance and length set by the membrane size. In this sense it is analogous to the bicontinuous cubic phase with long-range position and orientation order of curved membranes, and the novel but poorly understood P_{β}' "rippled" phase of multilayer membranes. In the P_{β}' phase, sandwiched between the commonly observed lamellar L_{α} (chain melted) and L_{β}' (chain ordered) phases of certain lecithin-water systems, the membrane modulation unit cell has the symmetry of a 2D monoclinic lattice (66–68).

Supplementary Material

Refer to Web version on PubMed Central for supplementary material.

ACKNOWLEDGEMENTS

REFERENCES

1. Rädler JO; Koltover I; Salditt T; Safinya CR: Structure of DNA-cationic liposome complexes: DNA intercalation in multilamellar membranes in distinct interhelical packing regimes. Science 1997, 275, 810–814. DOI: 10.1126/science.275.5301.810. [PubMed: 9012343]

2. May S; Ben-Shaul A: DNA-lipid complexes: stability of honeycomb-like and spaghetti-like structures. Biophys. J. 1997, 73, 2427–2440. DOI: 10.1016/S0006-3495(97)78271-7. [PubMed: 9370436]

3. Koltover I; Salditt T; Rädler JO; Safinya CR: An inverted hexagonal phase of cationic liposome-DNA complexes related to DNA release and delivery. Science 1998, 281, 78–81. DOI: 10.1126/science.281.5373.78. [PubMed: 9651248]

4. O'Hern CS; Lubensky TC: Sliding Columnar Phase of DNA-Lipid Complexes. Phys. Rev. Lett. 1998, 80, 4345–4348. DOI: 10.1103/PhysRevLett.80.4345.

5. Golubovi L; Golubovi M: Fluctuations of Quasi-Two-Dimensional Smectics Intercalated between Membranes in Multilamellar Phases of DNA-Cationic Lipid Complexes. Phys. Rev. Lett. 1998, 80, 4341–4344. DOI: 10.1103/PhysRevLett.80.4341.

6. Harries D; May S; Gelbart WM; Ben-Shaul A: Structure, Stability, and Thermodynamics of Lamellar DNA-Lipid Complexes. Biophys. J.1998, 75, 159–173. DOI: 10.1016/S0006-3495(98)77503-4. [PubMed: 9649376]

7. Bruinsma R: Electrostatics of DNA-cationic lipid complexes: isoelectric instability. Eur. Phys. J. B 1998, 4, 75–88. DOI: 10.1007/s100510050353.

8. Bruinsma R; Mashl J: Long-range electrostatic interaction in DNA-cationic lipid complexes. Europhys. Lett. 1998, 41, 165–170. DOI: 10.1209/epl/i1998-00125-0.

9. Golubovi L; Lubensky TC; O'Hern CS: Structural properties of the sliding columnar phase in layered liquid crystalline systems. Phys. Rev. E 2000, 62, 1069–1094. DOI: 10.1103/PhysRevE.62.1069.

10. Safinya CR: Structures of lipid-DNA complexes: Supramolecular assembly and gene delivery. Curr. Opin. Struct. Biol. 2001, 11, 440–448. DOI: 10.1016/S0959-440X(00)00230-X. [PubMed: 11495736]

11. Ewert KK; Evans HM; Zidovska A; Bouxsein NF; Ahmad A; Safinya CR: A columnar phase of dendritic lipid-based cationic liposome-DNA complexes for gene delivery: Hexagonally ordered cylindrical micelles embedded in a DNA honeycomb lattice. J. Am. Chem. Soc. 2006, 128, 3998–4006. DOI: 10.1021/ja055907h. [PubMed: 16551108]

12. Bouxsein NF; McAllister CS; Ewert KK; Samuel CE; Safinya CR: Structure and gene silencing activities of monovalent and pentavalent cationic lipid vectors complexed with siRNA. Biochemistry 2007, 46, 4785–4792. DOI: 10.1021/bi062138l. [PubMed: 17391006]

13. Leal C; Bouxsein NF; Ewert KK; Safinya CR: Highly Efficient Gene Silencing Activity of siRNA Embedded in a Nanostructured Gyroid Cubic Lipid Matrix. J. Am. Chem. Soc. 2010, 132, 16841–16847. DOI: 10.1021/ja1059763. [PubMed: 21028803]

14. Bouxsein NF; Leal C l.; McAllister, C. S.; Ewert, K. K.; Li, Y.; Samuel, C. E.; Safinya, C. R.: Two-Dimensional Packing of Short DNA with Nonpairing Overhangs in Cationic Liposome-DNA Complexes: From Onsager Nematics to Columnar Nematics with Finite-Length Columns. J. Am. Chem. Soc. 2011, 133, 7585–7595. DOI: 10.1021/ja202082c. [PubMed: 21520947]

15. Leal C; Ewert KK; Bouxsein NF; Shirazi RS; Li Y; Safinya CR: Stacking of short DNA induces the gyroid cubic-to-inverted hexagonal phase transition in lipid-DNA complexes. Soft Matter 2013, 9, 795–804. DOI: 10.1039/c2sm27018h. [PubMed: 23476712]

16. Kang M; Kim H; Leal C: Self-organization of nucleic acids in lipid constructs. Curr. Opin. Colloid Interface Sci. 2016, 26, 58–65. DOI: 10.1016/j.cocis.2016.09.006. [PubMed: 28496379]

17. Kang M; Leal C: Soft Nanostructured Films for Actuated Surface-Based siRNA Delivery. Adv. Funct. Mater. 2016, 26, 5610–5620. DOI: 10.1002/adfm.201600681.

18. Kim H; Sung J; Chang Y; Alfeche A; Leal C: Microfluidics Synthesis of Gene Silencing Cubosomes. ACS Nano 2018, 12, 9196–9205. DOI: 10.1021/acsnano.8b03770. [PubMed: 30081623]

19. Foldvari M; Chen DW; Nafissi N; Calderon D; Narsineni L; Rafiee A: Non-viral gene therapy: Gains and challenges of non-invasive administration methods. J. Controlled Release 2016, 240, 165–190. DOI: 10.1016/j.jconrel.2015.12.012.

20. Geinguenaud F; Guenin E; Lalatonne Y; Motte L: Vectorization of Nucleic Acids for Therapeutic Approach: Tutorial Review. ACS Chem. Biol. 2016, 11, 1180–1191. DOI: 10.1021/acschembio. 5b01053. [PubMed: 26950048]

21. Yin H; Kauffman KJ; Anderson DG: Delivery technologies for genome editing. Nat. Rev. Drug Discovery 2017, 16, 387–399. DOI: 10.1038/nrd.2016.280. [PubMed: 28337020]

22. Safinya CR; Ewert KK; Majzoub RN; Leal C: Cationic liposome-nucleic acid complexes for gene delivery and gene silencing. New J. Chem. 2014, 38, 5164–5172. DOI: 10.1039/c4nj01314j.

23. Yin H; Kanasty RL; Eltoukhy AA; Vegas AJ; Dorkin JR; Anderson DG: Non-viral vectors for gene-based therapy. Nat. Rev. Genet. 2014, 15, 541–555. DOI: 10.1038/nrg3763. [PubMed: 25022906]

24. Wang Y; Miao L; Satterlee A; Huang L: Delivery of oligonucleotides with lipid nanoparticles. Adv. Drug Delivery Rev. 2015, 87, 68–80. DOI: 10.1016/j.addr.2015.02.007.

25. Ewert KK; Kotamraju VR; Majzoub RN; Steffes VM; Wonder EA; Teesalu T; Ruoslahti E; Safinya CR: Synthesis of linear and cyclic peptide–PEG–lipids for stabilization and targeting of cationic liposome-DNA complexes. Bioorg. Med. Chem. Lett. 2016, 26, 1618–1623. DOI: 10.1016/j.bmcl. 2016.01.079. [PubMed: 26874401]

26. Majzoub RN; Ewert KK; Safinya CR: Cationic liposome–nucleic acid nanoparticle assemblies with applications in gene delivery and gene silencing. Philos. Trans. R. Soc., A 2016, 374 DOI: 10.1098/rsta.2015.0129.

27. Guo X; Huang L: Recent Advances in Nonviral Vectors for Gene Delivery. Acc. Chem. Res. 2012, 45, 971–979. DOI: 10.1021/ar200151m. [PubMed: 21870813]

28. Safinya CR; Ewert KK: Materials chemistry: Liposomes derived from molecular vases. Nature 2012, 489, 372–374. [PubMed: 22996547]

29. Bielke W; Erbacher C, Eds.: Nucleic Acid Transfection. Springer: Berlin, 2010.

30. Ewert K; Zidovska A; Ahmad A; Bouxsein N; Evans H; McAllister C; Samuel C; Safinya C: Cationic Liposome–Nucleic Acid Complexes for Gene Delivery and Silencing: Pathways and Mechanisms for Plasmid DNA and siRNA In Nucleic Acid Transfection, W. Bielke; C. Erbacher, Eds. Springer: Berlin, 2010; pp. 191–226. DOI: 10.1007/128_2010_70.

31. Huang L; Hung MC; Wagner E, Eds.: Non-Viral Vectors for Gene Therapy. 2nd ed.; Elsevier Academic Press: San Diego, 2005.

32. Ewert K; Ahmad A; Evans H; Safinya C: Cationic lipid-DNA complexes for non-viral gene therapy: relating supramolecular structures to cellular pathways. Expert Opin. Biol. Ther. 2005, 5, 33–53. DOI: 10.1517/14712598.5.1.33. [PubMed: 15709908]

33. Young SWS; Stenzel M; Jia-Lin Y: Nanoparticle-siRNA: A potential cancer therapy? Crit. Rev. Oncol. 2016, 98, 159–169. DOI: 10.1016/j.critrevonc.2015.10.015.

34. Ozcan G; Ozpolat B; Coleman RL; Sood AK; Lopez-Berestein G: Preclinical and clinical development of siRNA-based therapeutics. Adv. Drug Delivery Rev. 2015, 87, 108–119. DOI: 10.1016/j.addr.2015.01.007.

35. Rupaimoole R; Slack FJ: MicroRNA therapeutics: towards a new era for the management of cancer and other diseases. Nat. Rev. Drug Discovery 2017, 16, 203–222. DOI: 10.1038/nrd.2016.246. [PubMed: 28209991]

36. Guan S; Rosenecker J: Nanotechnologies in delivery of mRNA therapeutics using nonviral vector-based delivery systems. Gene Ther. 2017, 24, 133–143. DOI: 10.1038/gt.2017.5. [PubMed: 28094775]

37. Wan C; Allen TM; Cullis PR: Lipid nanoparticle delivery systems for siRNA-based therapeutics. Drug Delivery Transl. Res. 2014, 4, 74–83. DOI: 10.1007/s13346-013-0161-z.

38. Gindy ME; Leone AM; Cunningham JJ: Challenges in the pharmaceutical development of lipid-based short interfering ribonucleic acid therapeutics. Expert Opin. Drug Delivery 2012, 9, 171–182. DOI: 10.1517/17425247.2012.642363.

39. Gindy ME; DiFelice K; Kumar V; Prud'homme RK; Celano R; Haas RM; Smith JS; Boardman D: Mechanism of Macromolecular Structure Evolution in Self-Assembled Lipid Nanoparticles for siRNA Delivery. Langmuir 2014, 30, 4613–4622. DOI: 10.1021/la500630h. [PubMed: 24684657]

40. Pecot CV; Calin GA; Coleman RL; Lopez-Berestein G; Sood AK: RNA interference in the clinic: challenges and future directions. Nat. Rev. Cancer 2011, 11, 59–67. [PubMed: 21160526]

41. Lares MR; Rossi JJ; Ouellet DL: RNAi and small interfering RNAs in human disease therapeutic applications. Trends Biotechnol. 2010, 28, 570–579. DOI: 10.1016/j.tibtech.2010.07.009. [PubMed: 20833440]

42. Leal C; Ewert KK; Shirazi RS; Bouxsein NF; Safinya CR: Nanogyroids Incorporating Multivalent Lipids: Enhanced Membrane Charge Density and Pore Forming Ability for Gene Silencing. Langmuir 2011, 27, 7691–7697. DOI: 10.1021/la200679x. [PubMed: 21612245]

43. Gene Thera py Clinical Trials Worldwide. The Journal of Gene Medicine clinical trial site. http://www.wiley.com/legacy/wileychi/genmed/clinical/ (accessed August, 2019).

44. Ginn SL; Amaya AK; Alexander IE; Edelstein ML; Abedi MR: Gene therapy clinical trials worldwide to 2017 – an update. J. Gene Med. 2018, 2018;20:e3015. 10.1002/jgm.3015

45. Salditt T; Koltover I; Rädler JO; Safinya CR: Two-dimensional smectic ordering of linear DNA chains in self-assembled DNA-cationic liposome mixtures. Phys. Rev. Lett. 1997, 79, 2582–2585.

46. Salditt T; Koltover I; Rädler JO; Safinya CR: Self-assembled DNA-cationic-lipid complexes: Two-dimensional smectic ordering, correlations, and interactions. Phys. Rev. E 1998, 58, 889–904.

47. Nakata M; Zanchetta G; Chapman BD; Jones CD; Cross JO; Pindak R; Bellini T; Clark NA: End-to-End Stacking and Liquid Crystal Condensation of 6– to 20–Base Pair DNA Duplexes. Science 2007, 318, 1276–1279. DOI: 10.1126/science.1143826. [PubMed: 18033877]

48. Zanchetta G; Bellini T; Nakata M; Clark NA: Physical Polymerization and Liquid Crystallization of RNA Oligomers. J. Am. Chem. Soc. 2008, 130, 12864–12865. DOI: 10.1021/ja804718c. [PubMed: 18774799]

49. Artzner F; Zantl R; Rapp G; Rädler JO: Observation of a Rectangular Columnar Phase in Condensed Lamellar Cationic Lipid-DNA Complexes. Phys. Rev. Lett. 1998, 81, 5015–5018. DOI: 10.1103/PhysRevLett.81.5015.

50. Koynova R; MacDonald RC: Columnar DNA Superlattices in Lamellar o-Ethylphosphatidylcholine Lipoplexes: Mechanism of the Gel-Liquid Crystalline Lipid Phase Transition. Nano Lett. 2004, 4, 1475–1479. DOI: 10.1021/nl049191k.

51. McManus JJ; Rädler JO; Dawson KA: Observation of a Rectangular Columnar Phase in a DNA–Calcium–Zwitterionic Lipid Complex. J. Am. Chem. Soc. 2004, 126, 15966–15967. DOI: 10.1021/ja046105+. [PubMed: 15584722]

52. Mirkin CA; Letsinger RL; Mucic RC; Storhoff JJ: A DNA-based method for rationally assembling nanoparticles into macroscopic materials. Nature 1996, 382, 607–609. [PubMed: 8757129]

53. Elghanian R; Storhoff JJ; Mucic RC; Letsinger RL; Mirkin CA: Selective Colorimetric Detection of Polynucleotides Based on the Distance-Dependent Optical Properties of Gold Nanoparticles. Science 1997, 277, 1078–1081. DOI: 10.1126/science.277.5329.1078. [PubMed: 9262471]

54. Nykypanchuk D; Maye MM; van der Lelie D; Gang O: DNA-guided crystallization of colloidal nanoparticles. Nature 2008, 451, 549–552. DOI: 10.1038/nature06560. [PubMed: 18235496]

55. Maye MM; Nykypanchuk D; van der Lelie D; Gang O: A Simple Method for Kinetic Control of DNA-Induced Nanoparticle Assembly. J. Am. Chem. Soc. 2006, 128, 14020–14021. DOI: 10.1021/ja0654229. [PubMed: 17061872]

56. Chung PJ; Song C; Deek J; Miller HP; Li Y; Choi MC; Wilson L; Feinstein SC; Safinya CR: Tau mediates microtubule bundle architectures mimicking fascicles of microtubules found in the axon initial segment. Nat. Commun. 2016, 7, 12278 DOI: 10.1038/ncomms12278. [PubMed: 27452526]

57. Deek J; Chung PJ; Kayser J; Bausch AR; Safinya CR: Neurofilament sidearms modulate parallel and crossed-filament orientations inducing nematic to isotropic and re-entrant birefringent hydrogels. Nat. Commun. 2013, 4, 2224 DOI: 10.1038/ncomms3224. [PubMed: 23892390]

58. Beck R; Deek J; Choi MC; Ikawa T; Watanabe O; Frey E; Pincus P; Safinya CR: Unconventional Salt Trend from Soft to Stiff in Single Neurofilament Biopolymers. Langmuir 2010, 26, 18595–18599. DOI: 10.1021/la103655x. [PubMed: 21082794]

59. Horowitz VR; Janowitz LA; Modic AL; Heiney PA; Collings PJ: Aggregation behavior and chromonic liquid crystal properties of an anionic monoazo dye. Phys. Rev. E 2005, 72, 041710 DOI: 10.1103/PhysRevE.72.041710.

60. Koltover I; Salditt T; Safinya CR: Phase diagram, stability, and overcharging of lamellar cationic lipid- DNA self-assembled complexes. Biophys. J. 1999, 77, 915–924. DOI: 10.1016/S0006-3495(99)76942-0. [PubMed: 10423436]

61. Szleifer I; Kramer D; Ben-Shaul A; Roux D; Gelbart WM: Curvature Elasticity of Pure and Mixed Surfactant Films. Phys. Rev. Lett. 1988, 60, 1966–1969. DOI: 10.1103/PhysRevLett.60.1966. [PubMed: 10038189]

62. Safinya CR; Sirota EB; Roux D; Smith GS: Universality in interacting membranes: The effect of cosurfactants on the interfacial rigidity. Phys. Rev. Lett. 1989, 62, 1134–1137. [PubMed: 10039585]

63. Schiessel H; Aranda-Espinoza H: Electrostatically induced undulations of lamellar DNA-lipid complexes. Eur. Phys. J. E 2001, 5, 499–506. DOI: 10.1007/s101890170057.

64. Schiessel H: Bending of charged flexible membranes due to the presence of macroions. Eur. Phys. J. B 1998, 6, 373–380. DOI: 10.1007/s100510050563.

65. Helfrich W: Steric Interaction of Fluid Membranes in Multilayer Systems. Z. Naturforsch. A 1978, 33, 305–315. DOI: 10.1515/zna-1978-0308.

66. Wack DC; Webb WW: Synchrotron x-ray study of the modulated lamellar phase $P_\beta>$ in the lecithin-water system. Phys. Rev. A 1989, 40, 2712–2730. DOI: 10.1103/PhysRevA.40.2712.

67. Zasadzinski J; Schneir J; Gurley J; Elings V; Hansma P: Scanning tunneling microscopy of freeze-fracture replicas of biomembranes. Science 1988, 239, 1013–1015. DOI: 10.1126/science. 3344420. [PubMed: 3344420]

68. Sirota EB; Smith GS; Safinya CR; Plano RJ; Clark NA: X-ray scattering studies of aligned, stacked surfactant membranes. Science 1988, 242, 1406–1409. [PubMed: 17802136]
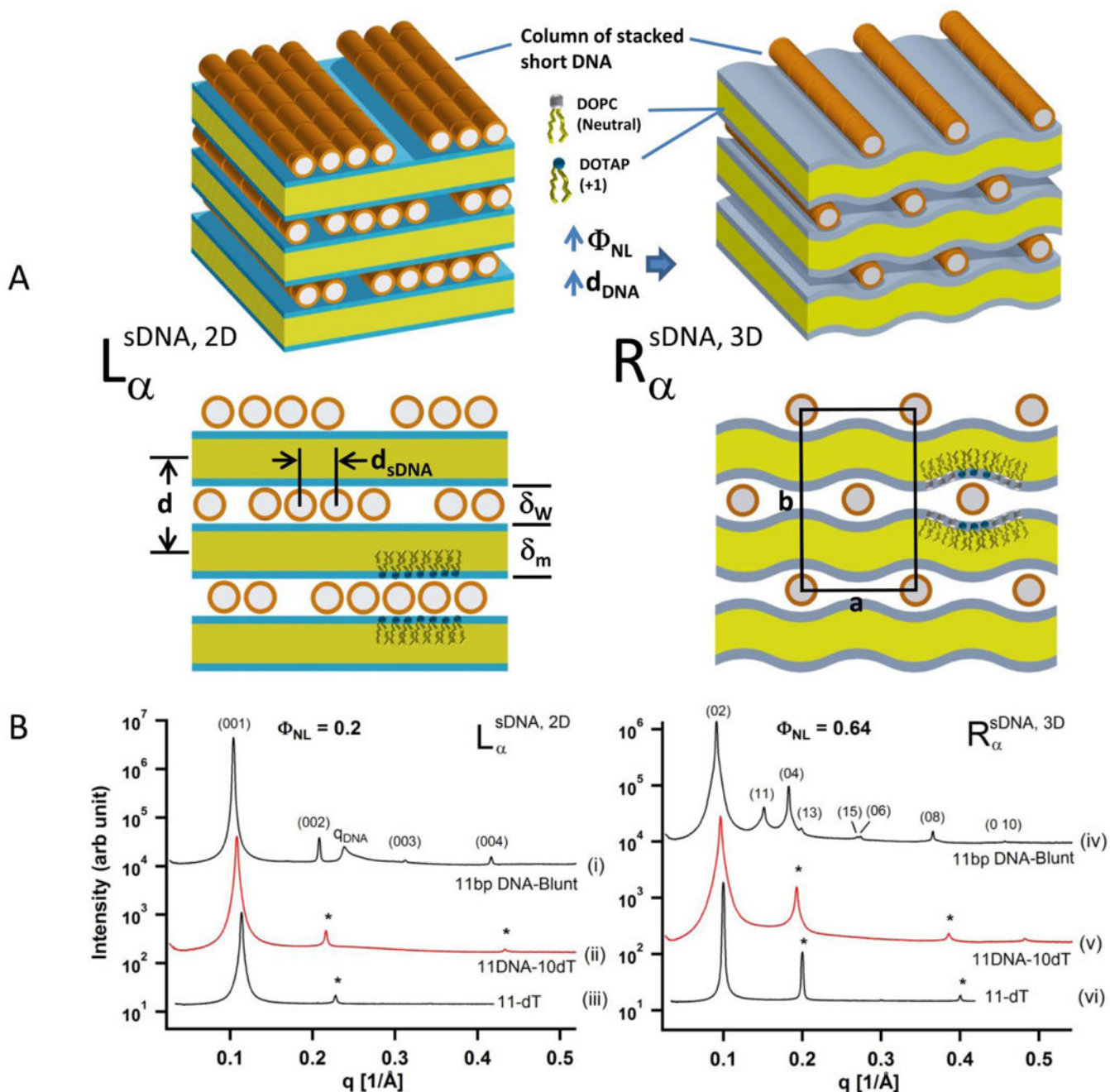
Figure 1.
2D ($L_\alpha^{sDNA,2D}$) and 3D columnar phases ($R_\alpha^{sDNA,3D}$) of stacked blunt short-DNA (sDNA) intercalated between fluid cationic lipid membranes (CL), revealed by synchrotron-based small angle x-ray scattering (SAXS). (A) LEFT: Graphic illustration of CL-sDNA complexes in the $L_\alpha^{sDNA,2D}$ phases. Formed at low mole fraction neutral lipid (Φ_{NL}) the stacked sDNA (depicted as short cylinders) sandwiched between cationic membranes form columns with a well defined DNA interaxial spacing in each layer, but without correlations from layer to layer. This phase is qualitativly similar to the previously observed 2D smectic like organization of long DNA in cationic liposome-DNA complexes (1,13,14). RIGHT:

Graphic illustration of CL-sDNA complexes in the $R_\alpha^{sDNA,3D}$ phase, which forms after Φ_{NL} is increased above a certain threshhold ($0.5 < \Phi_{NL}$ 0.75 for 11bp and 24bp sDNA, and $0.52 < \Phi_{NL}$ 0.75 for 48bp sDNA). In this phase, the sDNA rods across the bilayers exhibit strong correlations, forming a centered rectangular lattice with long range order. The stacked sDNA rods retain sliding degree of freedom along the helical axis. (B) (i) synchrotron x-ray scattering data of 11bp sDNA complexed with DOTAP/DOPC CLs for $\Phi_{NL} = 0.2$ at the isoelectric point. The presence of a series of peaks resulting from the memebrane stack and a highly asymmetric DNA 1D ordering peak is similar to what has been observed from CL-DNA complexes with long DNAs. The strong asymmetric lineshape is a direct indication of lack of the positional correlations of the 1D lattices across layers. This similarity to long CL-DNA data is evidence that the sDNA rods must be stacked end-to-end to form long columns. (ii) Diffraction data of 11DNA-10dT complexes at $\Phi_{NL} = 0.2$. The 11DNA-10dT has the same DNA core (11 bp, perfectly duplexed) but including 10 unpaired deoxythymidine nucleotides to each 3 ' end of the duplex. The introduction of dangling ends prevent end-to-end stacking and led to a very broad (barely visible) DNA correlation peak indicating that the DNA ordering is significantly hindered. (iii) Diffraction data from complexes made with a 11-base single-stranded homopolymer of deoxythymidine (11dT). There is no correlation peak from the 11dT ssDNA. (iv) Typical scattering profile of CL-sDNA complexes in the ordered $R_\alpha^{sDNA,3D}$ phase for 11bp sDNA at $\Phi_{NL} = 0.64$. The sharp peaks can be indexed to a centered rectangular columnar structure with 2D lattice parameters a (=center-to-center spacing of stacked sDNA columns=45.9 Å at $\Phi_{NL}=0.64$) and b (= 2*interlayer spacing d = 138.8 Å at $\Phi_{NL} = 0.64$) as shown in Fig.1 A (RIGHT). (v, vi) Comparison diffraction data for CL-DNA complexes with 11DNA-10dT and 11-base single stranded deoxythymidine (11dT), respectively. In both cases, the data show no peaks from ordered rectangular phase. This result confirms that end-to-end stacking of short blunt sDNA into long columns is required for forming both 2D ($L_\alpha^{sDNA,2D}$) and 3D columnar phases ($R_\alpha^{sDNA,3D}$).
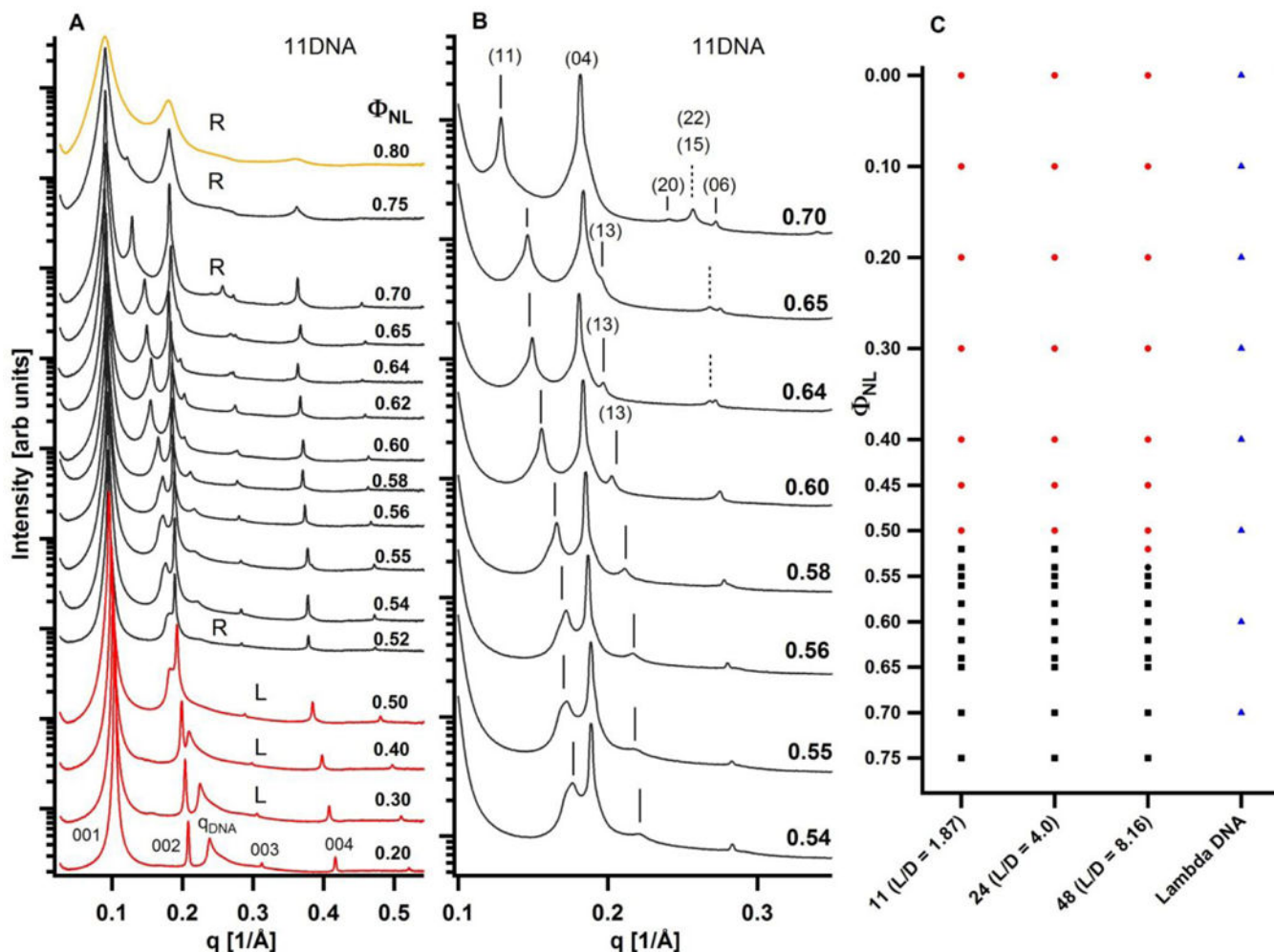
Figure 2.
Phase behavior of stacked sDNA columns in cationic liposome-sDNA complexes as a function of neutral lipid composition. (A) Complete series of synchrotron x-ray scattering profiles of CL-sDNA complexes for 11bp sDNA as a function of increasing Φ_{NL} covering the range from $\Phi_{NL} = 0.2$ to $\Phi_{NL} = 0.8$ (at the isoelectric point of the complex). (B) A plot of a subset of the x-ray profiles over a smaller q-range for Φ_{NL} between 0.54 and 0.70, where the onset of rectangular lattice peaks can be easily seen. (C) Phase diagram, compiled through analysis of x-ray diffraction data, for the $L_\alpha^{sDNA,2D}$ (indicated by black square) and $R_\alpha^{sDNA,3D}$ (indicated by red circle) phases as a function of Φ_{NL} for CL-sDNA complexes with 11DNA, 24DNA and 48DNA. All three lengths sDNA behavor similarly. The 4th line shows CL-DNA complexes formed with long λ–DNA, which remains in the L_α^C phase and do not exhibit a transition to the 3D columnar phase over the entire range of Φ_{NL} between 0 and 0.75.
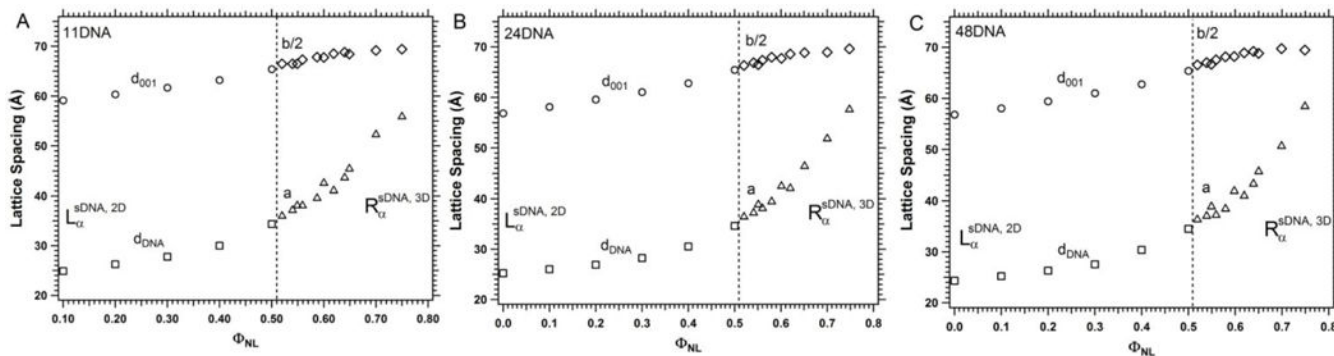
Figure 3.
Structural parameters derived from synchrotron x-ray scattering data from CL-sDNA complexes for 11bp, 24bp, and 48bp sDNA as a function of Φ_{NL} in the $L_\alpha^{sDNA,2D}$ and $R_\alpha^{sDNA,3D}$ phases. The vertical dotted lines mark the Φ_{NL} point above which $R_\alpha^{sDNA,3D}$ phase forms. Above the transition, the D_{DNA} spacing and lipid bilayer spacing d_{001} in the $L_\alpha^{sDNA,2D}$ phase become the lattice constants a and $b/2$ in the centered rectangular $R_\alpha^{sDNA,3D}$ phase. (A) Parameters for 11bp sDNA complexes. (B) Parameters for 24bp sDNA complexes. (C) Parameters for 48bp sDNA complexes.
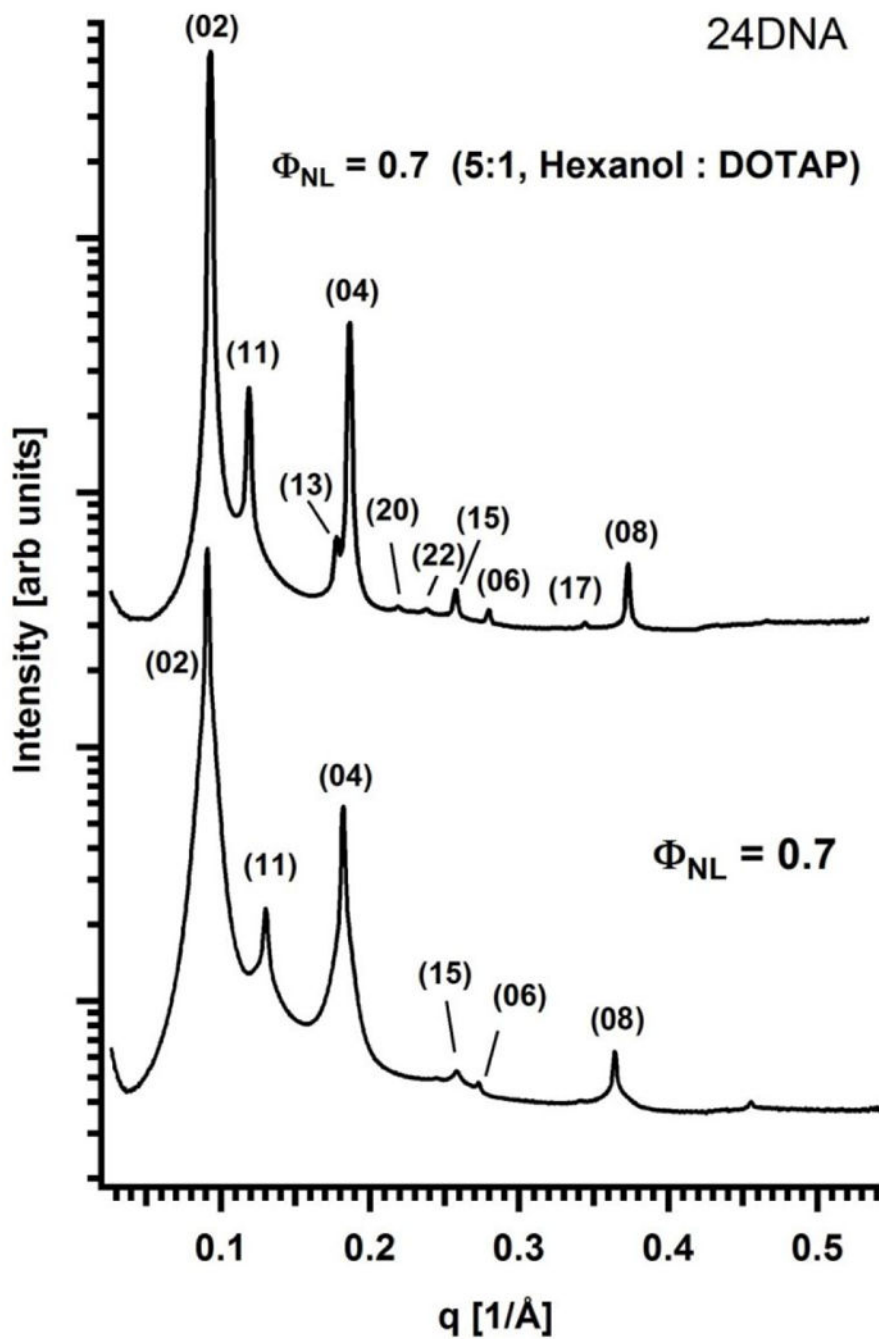
Figure 4.
Effect of membrane bending rigidity on the stability of the $R_\alpha^{sDNA,3D}$ phase. Bottom curve shows the x-ray scattering profile from 24bp complex in the $R_\alpha^{sDNA,3D}$ phase without any co-surfactant, whereas in the top curve, hexanol was added to the sample. The bending rigidity of the membrane is reduced by hexanol, which resulted in significantly sharper and more observable diffraction peaks from the rectangular lattice.
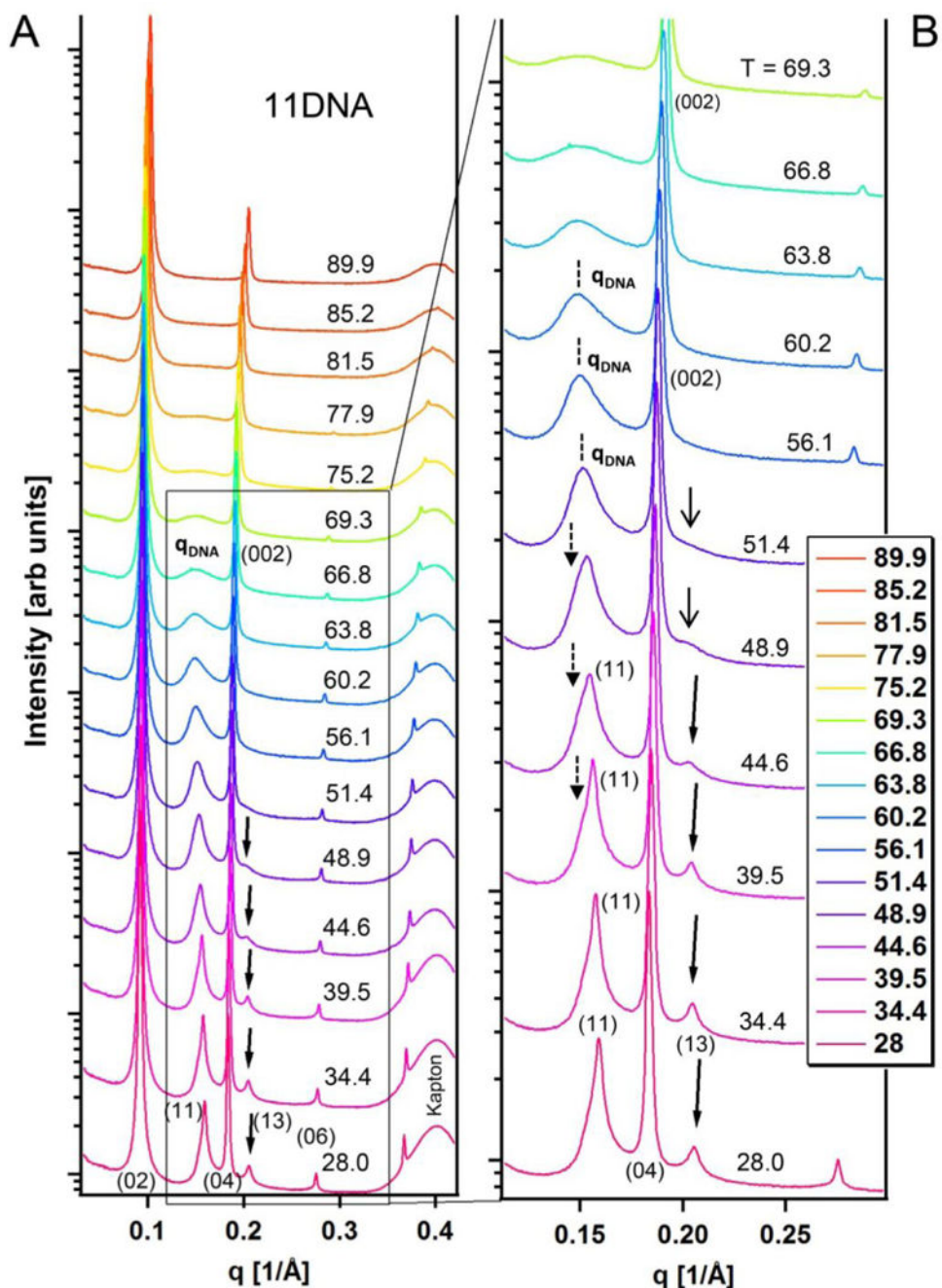
Figure 5.
Effect of temperature on stacked sDNA columns in cationic liposome-sDNA complexes. (A) X-ray scattering data plotted as a function of increasing temperature for CL-sDNA complexes with 11bp DNA in the $R_\alpha^{sDNA,3D}$ phase at $\Phi_{NL} = 0.6$. (B) An expanded view of the x-ray profiles over a smaller q- and temperature range. The (13) peak (see arrows) of the 3D columnar phase (melted in the 2D columnar phase) is used to track structural changes as function of temperature. Between 28 °C to 44.6 °C, where the (13) peaks are sharp (marked by slanted long arrows), the $R_\alpha^{sDNA,3D}$ phase dominates. At intermediate temperature range

T = 48.9 °C and 51.4 °C, the (13) peak is broad and indicate that there is only short range order. At higher temperatures (56.1 °C to ≈ 69.3 °C), the (13) peak is completely melted away and the diffraction pattern is indicative of the $L_\alpha^{sDNA,3D}$ phase. The complete vanishing of the sDNA correalation peak at T= 85.2 °C and 89.9 °C indicates that sDNA are no longer stacked end-to-end and are isotropically distributed between the memebrane layers.
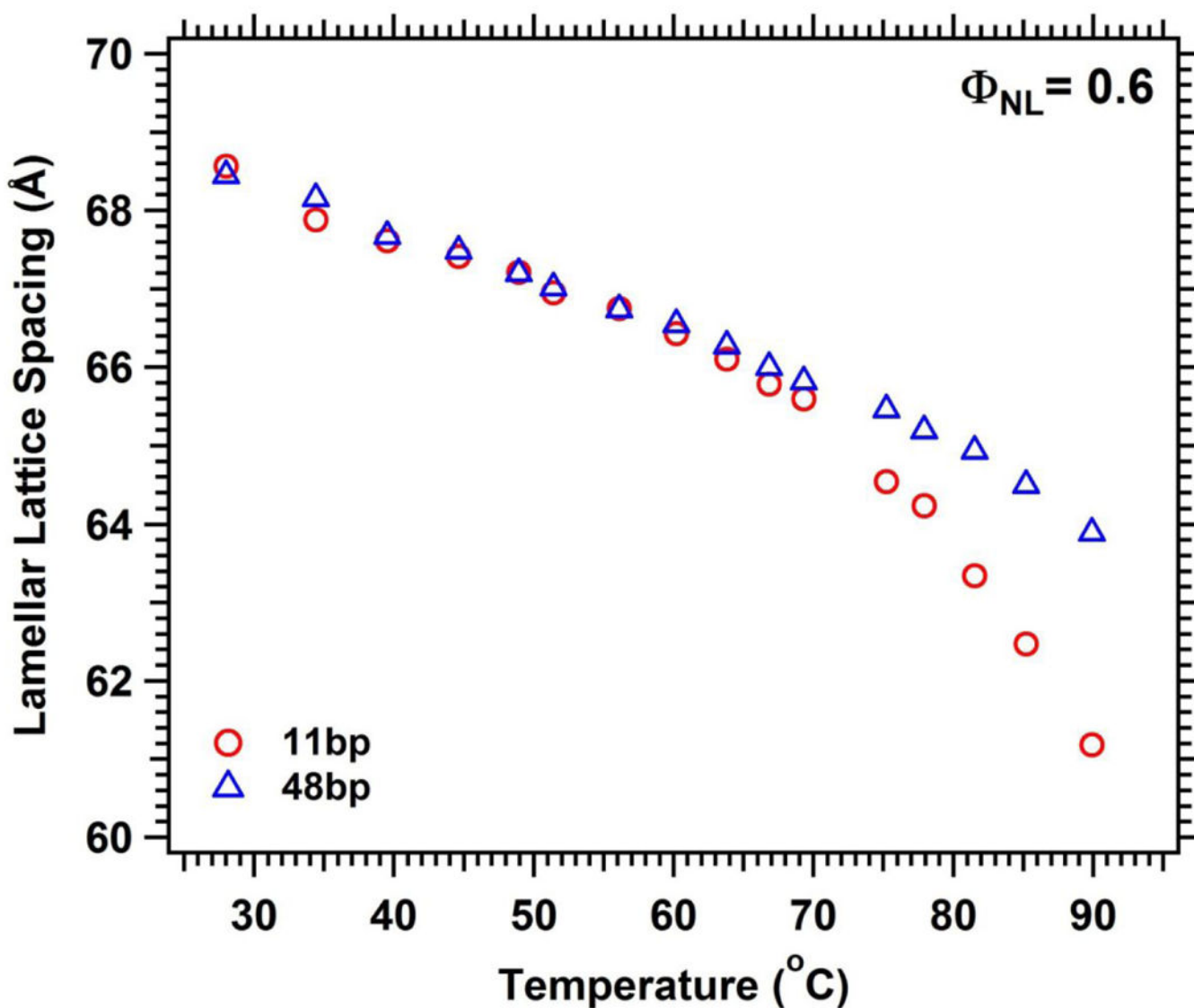
Figure 6.
Effects of temperature on lamellar lattice spacing (lipid bilayer plus the water layer containing sDNA) of CL-sDNA complexes at $\Phi_{NL} = 70.6$. The figure shows the spacing as a function of temperature for 11bp and 48bp sDNA. At T < 70 °C the two curves largely overlap, with d-spacing decreasing linearly with increasing T due to thermal contraction of lipid chains. At T >75 °C the d-spacing of complexes with 11bp sDNA decreases much faster with temperature indicative of the onset of denaturation of sDNA (i.e. where the water layer consists of a mixture of single starnd and double strand short DNA). The denaturation effect is much weaker for complexes with 48 bp sDNA.